# A "Twist" on the Interpretation of the Multifluorescence Patterns of DASPMI

Mireia Segado,* Enrico Benassi,* and Vincenzo Barone

Scuola Normale Superiore, Piazza dei Cavalieri 7, Pisa 56126, Italy

S *Supporting Information*

ABSTRACT: In this computational study, we describe the decay mechanism of DASPMI, providing robust and documented answers to some crucial questions of still open debates on the photophysical behavior of this cationic dye. After the initial excitation, the system evolves along a torsional motion, characterized by a quite flat potential energy surface, which crosses an intramolecular charge transfer (ICT) excited state with higher energy. A nonemissive twisted-ICT (TICT) minimum is populated, and this enhances the radiationless deactivation to the ground state. Additionally, during the twisting motion path toward the TICT minima, the system can emit in a quite wide range of angles, which should lead to a red shift of the locally excited (LE) emission and asymmetric broadening of fluorescence. This picture is fully supported by experimental evidence of the multifluorescence of DASPMI. Three twisted minima are found with different energies (namely, T1, T2, and T3). The extension of the work to charge properties shows that, in the GS, the positive charge of the molecule is mainly localized on the acceptor moiety (i.e., methyl-pyridinium), and after the excitation, the charge delocalizes over the whole molecule with a slight preference for the acceptor moiety. Because of the subsequent deactivation via twisting motions, the positive charge moves from the acceptor to the donor moiety (dimethylaminophenyl moiety) so that in TICT minima the positive charge is localized in the donor part. These large differences between charge localization in LE and TICT minima are responsible for a larger population of twisted forms in solvents of increasing polarity and the enhancement of radiationless deactivation.
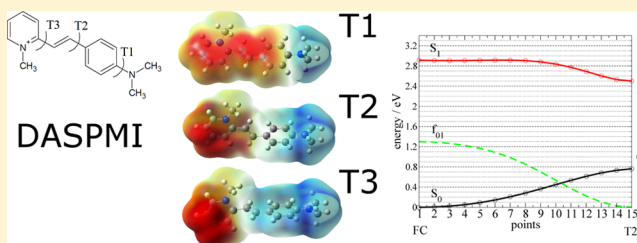
INTRODUCTION

Fluorescing donor−acceptor-substituted (push−pull) styryl dyes have widespread interest.[1−4] In particular, *o*-(*p*-dimethylamino-styryl)methylpyridinium cation (usually cited by the acronym DASPMI, see Scheme 1) is well-known to show a

Scheme 1. Chemical Sketch of DASPMI with Enumeration of Atoms and Definition of Dihedral Angles of Interest
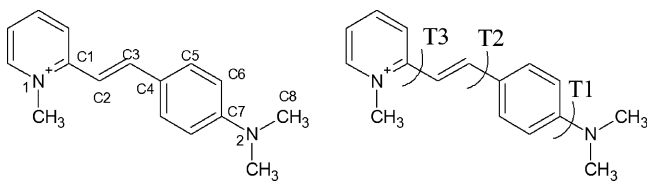
remarkable dependence of the fluorescence on the environment's polarity and viscosity. The environment (solvent) polarity dependence of DASPMI fluorescence makes it eligible for applications as a spectral sensitizer,[5] laser dye,[6] fluorescence probe,[7] and an efficient molecular system for electronics and nonlinear optics (NLO), in particular, for the second harmonic generation (SHG).[8,9] DASPMI also exhibits a strong charge reorganization upon excitation,[10] enlarging its possible medical applications as a fluorescence probe for neurons[11] or for detecting differences in the membrane potentials of biological systems. Conversely, regarding environmental viscosity depend-

ence of the fluorescence, DASPMI is also suitable for applications for the design of new smart materials, polymers, and in analytical chemistry (e.g., for detecting the micro-heterogeneity of the environment in confining media).[12,13]

Photophysics and photochemistry of DASPMI have been widely investigated with stationary fluorescence and pulse radiolysis, showing that the presence of a one electron-donating dimethylamino group in styryl-methylpyridinium dye reduces the *trans* → *cis* photoisomerization quantum yield and slightly enhances the fluorescence quantum yield with respect to nonsubstituted dimethylamino dye (from 70[14] to 8%[15] at room temperature). According to Rettig and co-workers[16] fluorescence competes with radiationless deactivation via trans conformations, the latter process being the main competing fluorescence deactivation path. There are two possible photo-chemical deactivation channels: nonradiative decay through single-bond twisting, which does not lead to a distinguishable photoisomer, and an alternative decay through double bond twisting leading to trans→ cis photoisomerization. A study comparing the photophysical behavior of bridged and unbridged styril dyes,[16] for which the possible torsion coordinates were blocked, shows that the photoisomerization process is more than 1 order of magnitude slower than single-

bond twisting for these compounds and is only observed in the compound where both T2 and T3 single bonds are bridged, thus pointing out the high photostability and absence of photoisomerization for these dyes.

Solvent polarity influences the spectroscopic behavior of DASPMI. In particular, positive solvatochromism, negligible or slightly positive fluosolvatochromism, and solvent dependence of the excited state (ES) dynamics are reported and discussed in the literature.[17−22] Photophysical investigations show a complex multifluorescence behavior within time-dependent Stokes shift dynamics whose origin is still unknown. Time-resolved picosecond fluorescence experiments assigned the blue part of the emission spectrum to species fluorescing from the locally excited (LE) state,[23] going beyond the common belief that a two-state fluorescence must be reflected by a two-band steady state emission spectrum. In a recent paper,[24] the excited-state dynamics of DASPMI were further investigated by ultrafast transient absorption spectroscopy. In moderately polar solvents, the charge displacement was found to be slower than the solvent rearrangement (CT controlled), whereas in polar solvents, the situation is reversed (solvent controlled) and a fast barrierless relaxation toward the final ICT state occurs.

Although the role of an intramolecular charge transfer (ICT) ES in the relaxation of DASPMI is so far accepted in the literature,[11,25,26] its exact electronic nature and formation mechanism are not yet clear. The reaction scheme of the ESs of DASPMI was first proposed by Formherz et al.[11,25] An ICT state is involved in the ES reaction path, leading to strong solvent-dependent dynamics. Within this picture, only an LE ES and twisted ICT (TICT) ES are considered for the potential energy hyper-surface (PES) (two-state model, Scheme 2a).

Scheme 2. Schematic Illustration of the Singlet ES and Ground State (GS) PESs According to (a) Two-State Model[11,25] and (b) Three-State Model[23a]

Two-state model[a]   Three-state model[b]
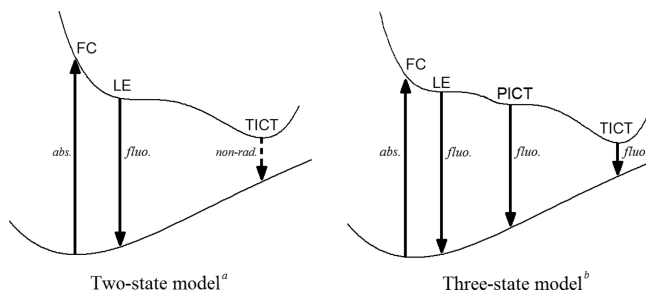
[a]Franck−Condon (FC), locally excited (LE), planar intramolecular charge transfer (PICT), and twisted intramolecular charge transfer (TICT) states.

This scheme is widely accepted, notwithstanding a recent study employing time- and space-correlated single-counting spectroscopical techniques,[23] which has proposed a different interpretation of the phenomena through a three-state model, which accounts for LE, Planar ICT (PICT), and TICT ESs in this order (three-state model, Scheme 2b). Unlike other donor−acceptor systems,[27] TICT of DASPMI is accepted to be nonradiative,[26] although the TICT state is the main character-istic of dual fluorescence for these kinds of system. Thus, the controversy about the PICT and/or TICT implication in the deactivation path is still unresolved.

Remarkable efforts have been spent on revealing the rotational motion involved in $S_1 \rightarrow S_0$ deactivation via ICT.

Mesurements at different viscosity conditions show non-radiative relaxation via large amplitude motions, but due to the possibility of different large twisting motions for DASPMI, these measurements do not enable localization of the specific coordinate. On the basis of semi-empirical calculations, Rettig et al.[26] proposed that the torsions around the $C_3−C_4$ bond (involving the dimethylaminophenyl, T2 in Scheme 1) and around the $C_1−C_2$ bond (involving methyl-pyridinium, T3 in Scheme 1) are the most favored ones with respect to that commonly accepted for these kinds of donor−acceptor systems,[28] i.e., around the $C_7−N_2$ bond (the dimethylamino group, T1 in Scheme 1). However, on the basis of (TD)B3LYP/3-21G calculations, T3 has been recently suggested[29] to be the only possible torsion motion involved in the $S_1 \rightarrow S_0$ deactivation.

Additionally, a burning controversy is still in progress regarding the localization of the positive charge when the TICT minimum is populated. On one hand, Rettig et al.[26] reported the localization of the positive charge on the donor moiety (dimethilamino group), whereas on the other hand, Carlotti et al.[29] localized the positive charge on the acceptor moiety (methyl-pyridinium ring).

Furthermore, experimental studies have attempted to identify the relevant torsion coordinate of the deactivation process. Glasbeek et al.[30] proposed the specific torsion by comparing the photophysical behavior of a series of analogues bridged and unbridged styril dyes for which the possible torsion coordinates were blocked through alkyl bridges between moieties involved in the possible torsion. The results of this study show that, as long as the dye has at least one unbridged T2 or T3 single bond, the lifetimes are comparable to the unbridged analogue, whereas when both T2 and T3 are bridged, the lifetimes lengthen, suggesting that the single T2 and T3 torsions allow an effective nonradiative deactivation. On the same track, recent additional experiments of submolecular spatial resolution by time-resolved SHG at liquid−liquid interfaces[31] on two aminostilbazolium iodide dyes (viz. 4-(4-(dibutylamino)styryl)-N-methylpyridinium iodide and 4-(4-(dihexadecylamino)-styryl)-N-methylpyridinium iodide) have revealed that the dependence on the viscosity predominantly involves the T2 torsion and assigns it as the main mode associated with the nonradiative deactivation.

Photophysical investigations of DASPMI show a complex multifluorescence behavior within time-dependent Stokes' shift dynamics, whose origin is still unknown. Time-resolved picosecond fluorescence experiments assign the blue part of the emission spectrum to species fluorescing from the LE state,[23] going beyond the classical picture of two-state → two-band model in the dual fluorescence. Recently, complementary femtosecond measurements, carried out to prove fast decay processes compared to fluorescence lifetimes (depending on solvent and viscosity),[29,30,32] have noticed three-time decays attributed to the solvent (τ_1), decay of LE (τ_2), and decay of ICT (τ_3), in this order.

From the comparison of the steady-state emission maximum band with the three-component stimulated emission obtained by femtosecond investigation, we evince that the maximum of the steady state fluorescence is between the second (τ_2) and third (τ_3) components. This is a relevant interpretation of the multifluorescence patterns of DASPMI, which still need to be confirmed by high-level theoretical calculations. To the best of our knowledge, no theoretical paper to date has been devoted to explaining the time-dependent Stokes' shift dynamics.

B

To summarize, the major questions concerning the complex behavior of DASPMI that still remain unanswered are

- what is the model that should be adopted: the two-state (LE/ICT) model or the three-state (LE/PICT/TICT) model?
- where does the charge localize after excitation, and during the deactivation dynamics?
- what is the origin of multifluorescence?

Most of the issues that have been raised in ∼30 years of experimental and theoretical investigations are probably due to the fact that the study of DASPMI seems to be particularly challenging from both an experimental and computational point of view. In particular, there are several features of this sytem that concur to make the theoretical investigation difficult: (a) DASPMI is a middle-large sized, charged chromophore; (b) the existence of both covalent and ICT states; (c) the large torsional motions in the ES dynamics; and lastly, (d) solvent effects, which require a refined treatment.

Thanks to the development of quantum chemical methods and computational facilities, only recently are state-of-the-art tools availabe to allow us to put effort toward a detailed and reliable description of the electronic features of such a nontrivial system, including also the effects due to the solvent. The considerations outlined above prompt us to deal with an accurate and sophisticate theoretical study on the photo-chemistry of DASPMI with particular interest toward the role played by the solvent. In this work, we employ different quantum chemical levels of theory, accepted as state-of-the-art techniques (vide infra), with the aim of (a) providing new insights into the decay mechanism of DASPMI, (b) separating the charge shift of different electronic states and their most probable torsions, and (c) clarifying the multifluorescence emission properties by obtaining the global deactivation path from the first FC excitation to the last deactivation of the GS. Furthermore, the comparison of earlier studies with our results validates the reliability of the designed methodology and enables us to suggest the enhancement of ICT and shortening of the ES lifetimes in high polarity solvents. The results of our approach seem to support the two-state model hypothesis. We propose that, after the initial excitation to the FC-LE state, the system evolves in a shallow PES with non-negligible emission probability. The structural deformations via T2 (and to a lesser extent T3) torsion finally lead to the population of a dark, twisted ICT state that thereafter relaxes to the GS. During this process, the charge flows from the methyl-pyridinium to the dimethylamino-phenyl moiety with a first spread of charge after the initial excitation to the LE state. This leads to different possible charge localizations when TICT is populated.

■ COMPUTATIONAL BACKGROUND AND DETAILS

General Remarks and Method Choice. It is well-known that the density functional theory (DFT) and time-dependent DFT (TD-DFT) methods give reliable descriptions of the geometry and electronic properties for the GS and ESs, both in the gas phase and in solution, when coupled with the polarizable continuum model (PCM).[33−36] However, for the system under investigation, because ICT states are involved, TD-DFT methodologies have to be employed with caution. In fact, according to some studies, an underestimation of the excitation energies, giving an incorrect ordering of state,[37] may occur when conventional density functionals not including long-range corrections are employed. Conversely, long-range corrected exchange correlation functionals (e.g., CAM-B3LYP[38]) give excellent CT excitation energies in comparison

to benchmark calculations.[37] Furthermore, CAM-B3LYP[38] is known to also provide an overall well-balanced description because no correlation is found between energy error and the degree of spatial overlap between the occupied and virtual orbitals involved in the excitation. This property is of high importance for the study of photochemistry of DASPMI because the evaluation of the possible involvement of twisting coordinates in the main reaction paths requires a balanced treatment of CT character along coupled and decoupled CT orbitals. DASPMI and its derivatives are challenging systems for computational methods due to their size and extended π-conjugated system such that the investigation of them requires a compromise between accuracy and computational cost. In this study, we perform an extended exploration in order to select a level of theory able to meet the above requirements.

GS Geometry Optimization and TD Properties. The molecular geometry of DASPMI was fully optimized at the DFT CAM-B3LYP/6-31+G* level. The properties of the first five singlet excited electronic states, the wave functions, and the electronic spectra were investigated at TD-DFT and (for CAM-B3LYP/6-31+G* only) the TDA-DFT level. We have compared the TD-DFT results obtained employing different functionals. In particular, we have chosen hybrid (viz. B3LYP,[39,40] PBE0,[41] and M06-2X[42]) and long-range corrected (viz. CAM-B3LYP,[38] LC-ωPBE,[43] and ωB97X)[44] coupled with the 6-31+G* basis set. The CAM-B3LYP funcional was also tested with the SNSD[45] basis set.

The accuracy of the excitation energies and the correctness of the order of ESs are quantified by comparing the TD(A)-DFT results with multiconfigurational Complete Active Space SCF (CASSCF)[46] in conjunction with Multi-State CAS second order Perturbation Theory (MS-CASPT2)[47] and equation of motion second order coupled cluster (EOM-CC2)[48] results (vide infra).

Multireference Calculations. The full valence π active space of DASPMI for CASSCF calculations is defined by 16 electrons in 15 molecular orbitals (MOs), i.e., (16,15). Without imposing symmetry constraints, such an active space would be prohibitive due to the enormous computational time required. Therefore, a smaller active space must be mandatorily chosen, meaning that the occupied and virtual MOs of lowest and highest energy, respectively, had to be removed from the full active space (the details of the reduction of the active space are shown in Supporting Information section SI.1.1). Active spaces (12,12), (14,13), and (16,14) (accounting for 12, 14, and 16 electrons in 12, 13, and 14 MOs, respectively) were used in CASSCF calculations.

To incorporate the effect of the dynamic valence electron correlation of the relative energies of the lower ESs, we also ran CASPT2 calculations based on the CASSCF reference function. All CASPT2 calculations were performed using an imaginary level shift of 0.20 au, to avoid the incorporation of intruder states, and a standard value for IPEA shift of 0.25 au

Interaction of CASSCF states via dynamic correlation is taken into account with MS-CASPT2 treatment. CASSCF/CASPT2 calculations were carried out with an ANO-S basis set (4s3p1d for carbon and nitrogen atoms, and 2s1p for hydrogen atoms). The effect of the basis set was analyzed and reported in Section SI.3.

PES Exploration. Because of the middle-large dimensions of DASPMI, MS-CASPT2/CASSCF and EOM-CC2 computations would have had prohibitive computational costs for an extensive exploration of the PES. Therefore, such an
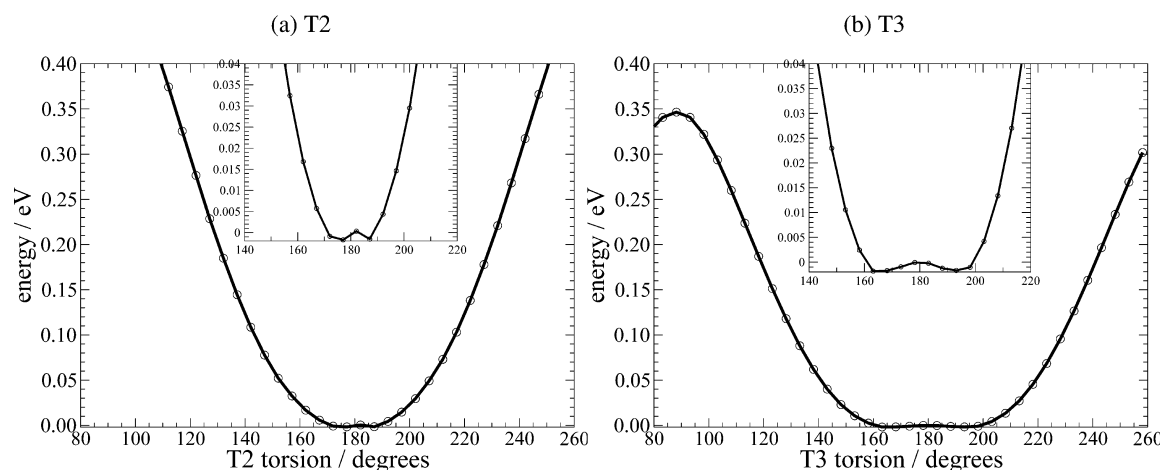
Figure 1. Relaxed GS PES scans around T2 (a) and T3 (b) torsions in vacuo.

exploration was performed at the TD-DFT CAM-B3LYP/6-31+G level, which enables us to obtain a reliable description of neutral and CT states.

The GS PES was analyzed by independent fully relaxed scanning of the T1, T2, and T3 dihedral angles around the σ-bonds around the equilibrium geometry values with a scan step of 5 degrees.

When necessary, minimum energy paths (MEP) and linearly interpolated internal reaction coordinate (LIIRC) paths were calculated between critical points of interest in several PESs to individuate a plausible ES population mechanism.

To refine the energies of $S1$ minima, we computed EOM-CC2 energies at CAM-B3LYP-optimized geometries. In PES exploration, CASSCF/CASPT2 methodology is not adopted because a nonfully active space would not ensure a balanced treatment between planar and twisted structures.

Electrostatic Properties and Solvent Treatment. The electric dipole moment for a charged species is undefined because it depends on the choice of the coordinate origin. However, in quantum and computational chemistry, a "working definition" is commonly assumed, which refers to the center of the nuclear charge of the system that, in our case, coincides with the center of mass.[49] We have computed μ for S_n ($n = 0, 1, \ldots 5$) at $(TD(A)-)DFT$ functionals used at the FC region, assuming the above-mentioned working definition.

Solvent effects were taken into account at the TD-DFT level by means of the implicit polarizable continuum model in its integral equation formalism (IEF-PCM).[34,35]

The excitation energies were calculated at the TD-DFT level by employing both the standard linear-response (LR) and the state-specific (SS) treatments of solvent effects at the minima located in vacuo both within the nonequilibrium (neq) and equilibrium (eq) solvation regimes, i.e., when only fast solvent degrees of freedom are in equilibrium with the ES electron density (neq) and at $t \rightarrow +\infty$, when the solvent is fully equilibrated with the solute density[36] LR-PCM is the standard used in TD-DFT/PCM calculations. However, in certain cases, LR could be not reliable when the molecule has charge transfer ESs or weak transitions are involved due to the underestimation of the energy of solvation between solvent and molecule.[50] In these cases, SS calculations provide more reliable and accurate ES energies. In the SS approach, the solvent reaction field is computed using the electron density of the state of interest, whereas in the LR approach, the energies are computed as

poles of the frequency dependent response function of the GS. Until now, the LR method has analytical gradients implemented in the *Gaussian* code whereas the SS method does not yet.

When we need to calculate the properties of the ESs in solution, we have to remember that the solvent responds in two ways to changes in the electronic state of the solute through solvent electron distribution polarization (rapid process) and solvent molecule reorientation (slow process). The former process requires a noneq calculation because it is too rapid for the solvent to respond (e.g., a vertical electronic excitation). On the contrary, the latter process requires an eq calculation, which describes a condition in which the solvent has (infinit) time to fully respond to solute changes (e.g., an ES geometry optimization). In the time frame between the absorption and the emission, the system is in an intermediate condition between the two regimes.

The PCM molecular cavity was built according to the Universal Force Field (UFF) radii within the value used in the last implementation of the PCM (based on a continuum surface charge formalism). Two solvents of different polarity were employed: dichloromethane (DCM) and acetonitrile (ACN). The standard values for the dielectric constants and refractive indexes were assumed (vide infra).

Quantum Chemical Codes. For DFT calculations, the *Gaussian*[51] package of programs was employed. CASSCF and CC2 calculations were performed using *Molcas*[52] and *Dalton*[53] codes.

RESULTS AND DISCUSSION

The photochemical process can be framed into three stages: the initial excitation, the immediately successive relaxation, and the subsequent secondary processes, all of which are affected by the environment. We have organized this section into four subsections. In the first subsection, related to the initial photoexcitation, we show natural and excitation energies of several ESs at the FC region. In the second subsection, the charge localization is analyzed in detail. In the third subsection, the stable structures found at the PES of the different ESs involved in the process and the possible reaction paths are proposed. In the fourth section, results concerning the solvent effects of all of the previous steps are discussed.

FC Region and ES Nature. The first aim is to locate the minimum energy relaxed geometry of DASPMI in the GS and

to calculate the energies of the ESs at this geometry in the FC region. GS geometry optimization and scans around T2 and T3 torsion coordinates were computed in vacuo at the DFT CAM-B3LYP/6-31+G* level (see Figure 3). Near the planar conformation minimum, the PES shows a quite broad *plateau* where torsions around the minimum are allowed. Assuming an (arbitrary) energy limit of 0.05 eV ($\approx$1 kcal/mol), ΔT2 $\approx$ 60 degs, and ΔT3 $\approx$ 80 degs. This means that in the GS the molecular structure shows a remarkable flexibility around both T2 and T3 (Figure 1).

The vertical ESs are labeled as reported in Figure 2, and the relative energies with respect to the GS are collected in Table 1.
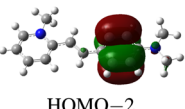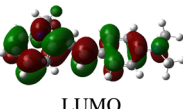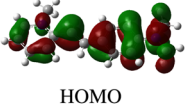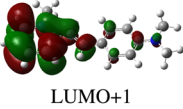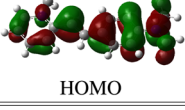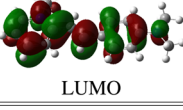
Label	from	to
ICT (A)	HOMO−2	LUMO
ICT (P)	HOMO	LUMO+1
LE	HOMO	LUMO

Figure 2. ES labeling with the most important molecular orbitals involved in transitions (from, to) and of lowest-lying ESs. E(HOMO − 2) = −11.47 eV; E(HOMO) = −9.35 eV ; E(LUMO) = −4.63 eV ; E(LUMO + 1)= −3.63 eV. Energies refer to the CAM-B3LYP/6-31+G* level.

Table 1. SS-CASPT2 (SS), MS-CASPT2 (MS), CC2, and TD-DFT/CAM-B3LYP (CAM) Excitation Energies ΔE and Oscillator Strengths (f) with an Active Space for CASSSCF of (16,14)

	ΔE (eV)				f		
state	SS	MS	CC2	CAM	MS	CC2	CAM
LE	2.57	2.57	2.54	2.91	1.52	1.40	1.30
ICT(P)	3.48	3.47	3.70	3.85	0.06	0.04	0.04
ICT(A)	4.15	4.16	4.32	4.41	0.08	0.00	0.00

The first singlet state (LE), which is the bright state, is mainly characterized by an excitation from HOMO to LUMO. The second ES (ICT(P)) involves a density transfer from the whole

molecule structure (HOMO) to the pyridil moiety (LUMO + 1). The third ES is characterized by charge delocalization from quinoidal π orbital of the dimethylamino-phenyl (HOMO − 2) to the whole molecular structure (LUMO). The charge (de)localization will be discussed in more detail in the Charge Localization section.

MS-CASPT2 and EOM-CC2 give similar results, showing the difference in excitation energy between both methods is less than 0.2 eV. Section SI.2 shows the vertical excitation energies and the oscillator strengths computed at the DFT level, employing different hybrid and long-range corrected functionals to compute vertical excitations (viz. B3LYP, CAM-B3LYP, PBE0, LC-ω PBE, M06-2X, and ωB97X). The evaluation of the reliability of these functionals to describe lowest-lying ESs of DASPMI was made by comparison with CASSCF/CASPT2 and EOM-CC2 results. For all the employed levels of theory, the prediction of energies shows the same ordering of low-lying ESs and the same nature. CAM-B3LYP and M06-2X give the best estimation of excitation energies in comparison with CASPT2 and EOM-CC2. PBE0 and MS-CASPT2 excitation energies are similar for LE, but PBE0 fails when describing ICT(P) and ICT(A) ESs, as is documented in previous studies.[37] Conversely, the agreement concerning the oscillator strengths is satisfactory for all of the tested functionals.

Taking these results into consideration, the support of previous studies on the reliability of CAM-B3LYP for ICT states, and the expensive computational effort required for a detailed exploration of the PESs at CASSCF/MS-CASPT2 or EOM-CC2 levels, we have chosen (TD-)DFT/CAM-B3LYP as the level of theory to inspect the PESs of GS and ESs.

Charge Localization. In this section, we analyze how the charge distributes when GS and ESs are populated. We chose to visualize the charge localization by calculating the electric dipole moments and by plotting the electrostatic potential maps (EPMs).

Figure 3 and Table 2 show information about the electric dipole moments. The CASSCF results refer to (16,14) active space (the ones calculated with (14,13) and (12,12) active spaces are shown in Table SI7). Concerning the electric dipole moment properties, CASSCF/CASPT2 and EOM-CC2 give almost coinciding results, whereas at DFT/CAM-B3LYP, LE shows a dramatic change in the electric dipole moment in comparison with those of CAS, MS, and CC2 (see Figure 3) despite the low-lying ESs being characterized by remarkably similar electronic properties at DFT, CASSCF/CASPT2, and EOM-CC2. DFT and CASSCF EPMs results referring to FC are depicted in Figure 4. For GS, both these methods show a
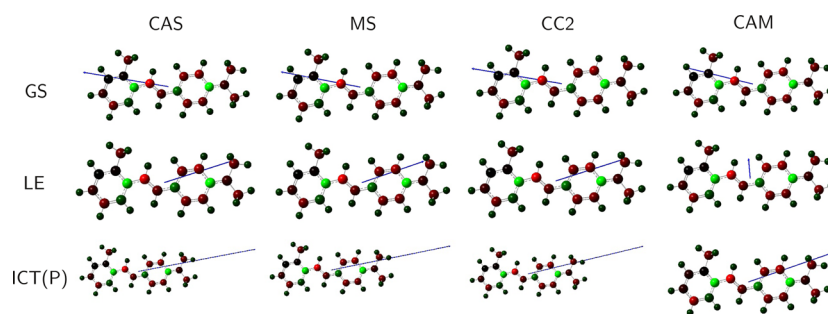
Figure 3. Electric dipole moments of low-lying ground and ESs at FC geometry at different levels of theory: CASSCF(16,14) (CAS), MS-CASPT2(16,14) (MS), EOM-CC2 (CC2), and DFT CAM-B3LYP (CAM).

Table 2. SS-CASPT2 (SS), MS-CASPT2 (MS), CAM-B3LYP (CAM), and EOM-CC2 (CC2) Dipole Moment Moduli μ for GS and ES and Angles θ Formed by the Directions of ES and the GS Dipole Moments with Active space (16,14)

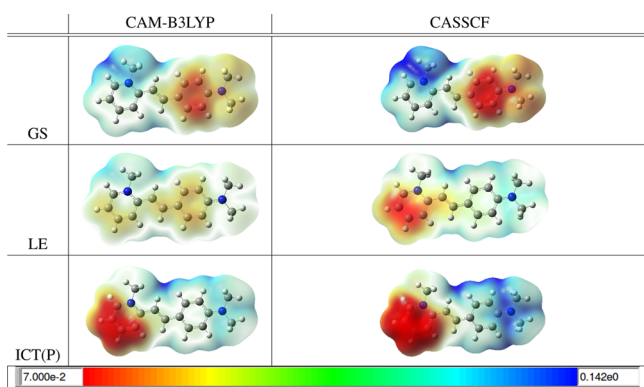|	μ (D), θ (degs)			
states	CAS	MS	CC2	CAM
GS	7.01	6.30	4.73	5.73
LE	5.35, 152.8	4.94, 150.2	5.58, 138.1	1.56, 72.0
ICT(P)	13.30, 159.7	12.92, 157.8	13.32, 145.5	7.77, 147.5

Figure 4. Electrostatic Potential Maps (EPM) for the GS, LE, and ICT states.

localization of the positive charge on the methyl-pyridinium moiety (in blue). In the case of LE, the positive charge is more evenly distributed over the whole molecular structure, more specifically at the DFT CAM-B3LYP level, the positive charge is almost delocalized and at CASSSCF is slightly localized on dimethylamino-phenyl moiety; in both the cases, it lowers the dipole moment with respect to the GS. In the case of the ICT(P) state, the positive charge (in blue in Figure 4) spreads from the methyl-pyridinium over the whole molecular system to the dimethylamino-phenyl moiety. The comparison between CAM-B3LYP and EOM-CC2 confirms the quantitative under-estimation of the amount of charge transferred at the TD-DFT level, as previously reported by Eriksen et al.[54]

In summary, the results show that several methods give the same *qualitative* description of the electronic structure of GS and ES (states described by the same electronic transitions). However, *quantitatively*, the amount of charge transferred during each transition is underestimated in the case of DFT/CAM-B3LYP with respect to CASSCF and CC2, which leads to a strong effect on the orientation (e.g., LE) and length (e.g., ICT(P)) of the electric dipole moment.

Because it is well-known that differences between GS and ES dipole moments correlate with solvatochromism, this result indicates that caution must be adopted in the treatment of solvent effects.

Reaction Paths. During the time evolution of a system over a PES through relaxation from one toward the nearest minimum, the effective reaching of a minimum depends on possible alternative processes competing with each other. If a minimum is populated, different types of processes could occur (e.g., fluorescence, internal conversion (IC) to GS, or population of other ES), each of those competes as a possible deactivation channel for the system. Below, we shall analyze the deactivation paths from FC, the minima of the PES, and the twisted motion paths. MS-CASPT2/CASSCF and EOM-CC2

computations would have had prohibitive computational costs for an extensive exploration of the PES; as a consequence, detailed exploration of the PES was performed at the TD-DFT CAM-B3LYP/6-31+G* level.

Seeking the Minima and Their Investigation. After initial vertical excitation from the GS to the FC region of S_1 (HOMO−LUMO), the system relaxes along its PES. Figure 5 shows the MEP computed from FC(S_1) at the CAM-B3LYP/
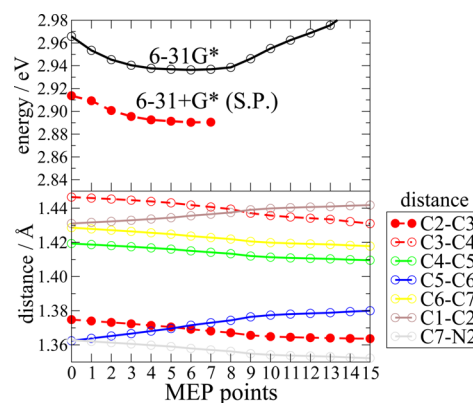

Figure 5. Minimum energy path (MEP) from FC(S_1) computed at the CAM-B3LYP/6-31G* level and single point calculations at CAM-B3LYP/6-31+G*. For each point, some C−C distances are depicted.

6-31G* level. Single point calculations were additionally done with a larger basis set including diffuse function 6-31+G*. From the static point of view of the DFT results, the system follows the gradient of the surface, which in this case makes the ES evolve toward a very flat surface leading to planar LE shallow minima (observed at the point number 7 with both basis sets).

To analyze how the geometrical parameters evolve during the relaxation along this PES, in the bottom panel of Figure 5, we also plotted some of the C−C distances for each point of the MEP. The C_2−C_3 central distance shortens, whereas the C_3−C_4 distance elongates. This could enhance the torsion along this coordinate in the first stages of the deactivation path.

Next, we aimed to find the low-lying minima of S_1. Table 3 collects the transition energies, the electric dipole moment, and

Table 3. Adiabatic Energy (ΔE_a), Vertical Energy (ΔE_{vert}), Electric Dipole Moment Modulus (μ), and Oscillator Strength (f) for the Optimized S_1 Minima

	CAM				CC2
minima	ΔE_a (eV)	ΔE_{vert} (eV)	μ (D)	f	ΔE_a (eV)
T1	2.92	1.94	10.25	0.000	
T2	2.50	1.74	10.47	0.000	2.37
T3	2.72	2.06	9.77	0.023	2.65
P3	3.53	3.28	7.03	0.238	
LE	2.89	2.85	1.53	1.255	2.48
FC(S_1)	2.91	2.91	1.56	1.300	2.54

the oscillator strength of the minimum identified at the DFT CAM-B3LYP level. Three kinds of minimum, related to as many twisted rotamers (T1, T2, and T3), are found for S_1. Another slightly twisted minimum with torsion T3, related to ICT(P), is also obtained, but it is higher in energy than the vertical absorption energy (0.62 eV), and thus, it could not be reached. Thus, we find from DFT results that the minimum corresponding to T2 is the most stable.

To refine the energies of S_1 minima, we performed EOM-CC2 calculations, keeping the above-mentioned S_1 geometries. These calculations confirm that T2 is the most stable minimum. CASSCF/CASPT2 methodology is not adopted in this step because a nonfully active space could not ensure a balanced treatment between planar and twisted structures.

Although from the analysis of the energy we could conclude that both LE and ICT minima might be populated, the oscillator strengths for the transition from the GS to the most stable T2 and T3 ICT states are negligible (0.00, 0.02) when compared to the GS → LE state (i.e., 1.255). This can be explained straightforwardly by evoking the overlap of the MOs describing the excitation to the ICT state, because when the charge is transferred, the orbitals are decoupled by the torsion coordinate such that the transition becomes overlap forbidden. Then, the emission from TICT minima might be observed only if this state has a long lifetime.

Charge properties show a strong dependence on the structural parameters. The EPM scheme allows us to imagine how the charge moves when the molecule twists and how it changes from the first excitation qualitatively. EPMs of T1, T2, and T3 minima are plotted in Figure 6. At different values of
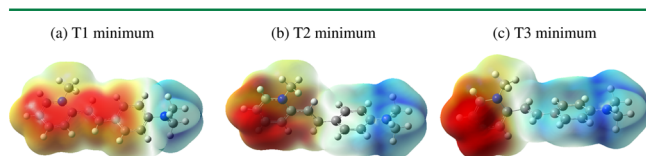

Figure 6. Mapped electrostatic potentials (MEPs) taken for TD-DFT CAM-B3LYP densities at different S_1 minima.

the torsional angle, we observe different charge localizations: on the out-of-ring amino group (T1), on the whole dimethylamino-phenyl group (T2), and on the methylamino styril group (T3).

Twisted Motion Paths. To focus our study only on the reactive channels of the S_1 PES, we need to account for several considerations: The LE state could be populated after the initial excitation, but the lowest energy minima of the S_1 surface correspond to the T2 and T3 states. Additionally, MEP from the FC region shows an enlarging of C−C distances involved in T2 and T3 torsions. Therefore, the evolution of these rotations from the FC region needs to be evaluated. Thus, its linear interpolation internal reaction coordinate (LIIRC) paths between FC and all three twisted minima are computed.

Figure 7 plots the PES profiles together with the oscillator strengths for the $S_1 \rightarrow$ GS transition as a function of the five intermediate points interpolated between FC and twisted minima. The profiles show that twist angles of 0 and 90 deg, corresponding to the LE (FC) and T2/T3 minima, respectively, are connected by a small rotation barrier (<0.5 meV), whereas for the twisting angles corresponding to LE (FC) and T1, the two minima are separated by a larger energy barrier (~0.31 eV).

In T2 and T3 twisting profiles, S_1 energy and oscillator strength undergo no appreciable change in a large range of twisting angles (from point number 1 to number 10, approximately) unlike GS, which is lower in energy because of the twisting coordinate. Thus, the LE state energy is not strongly affected by torsional distortions, leading to a shallow S_1 PES along points 1 to 10. Additionally, from point 12 at large T1, T2, and T3 torsion coordinates, the LE state crossing with an ICT state has a strong effect on the PES and its gradient. Concerning oscillator strengths, f smoothly tends to zero for the TICT minima but surprisingly has non-neglible values in a large interval of angles (its half value approximately corresponds to point number 12 of the paths).

All of these features should support a picture where the emission occurs from the intermediate twisted forms.

Solvent Role. As mentioned in the Introduction, DASPMI fluorescence shows a strong dependence on solvent polarity. Radiationless deactivation is also enhanced by increasing solvent polarity. With the aim of explaining this behavior, we studied the effects of two aprotic solvents with different polarities on the minima of GS and S_1 PES: dichloromethane (DCM; $\epsilon = 8.930$, $n^2 = 2.028346$) and acetonitrile (ACN; $\epsilon = 35.688$, $n^2 = 1.806874$).

Ground State. Relaxed scans along T2 and T3 torsion coordinates were computed for the GS geometry at the CAM-B3LYP/6-31+G*//PCM(UFF) level in two solvents of different polarity. From the scanning profiles (Figure 8), we evaluated the ranges of values accessible under an (arbitrary) energy barrier $\Delta E = 0.05$ eV (≈ 1 kcal/mol). These should be compared to those computed in vacuo (Figure 7). As it occurs in vacuo, the two selected solvents ΔT2 are also ~45 degs. On the contrary, T3 seems more sensitive to the presence of the solvation (in vacuo, ΔT3 ≈ 60 degs; in solvent, ΔT3 ≈ 80 degs; independent based on the choice of solvent). Thus, also in solvated phase, DASPMI still shows a peculiar flexibility in the GS around both T2 and T3. This is somehow a singular behavior because, in the case of dipolar compounds, they show
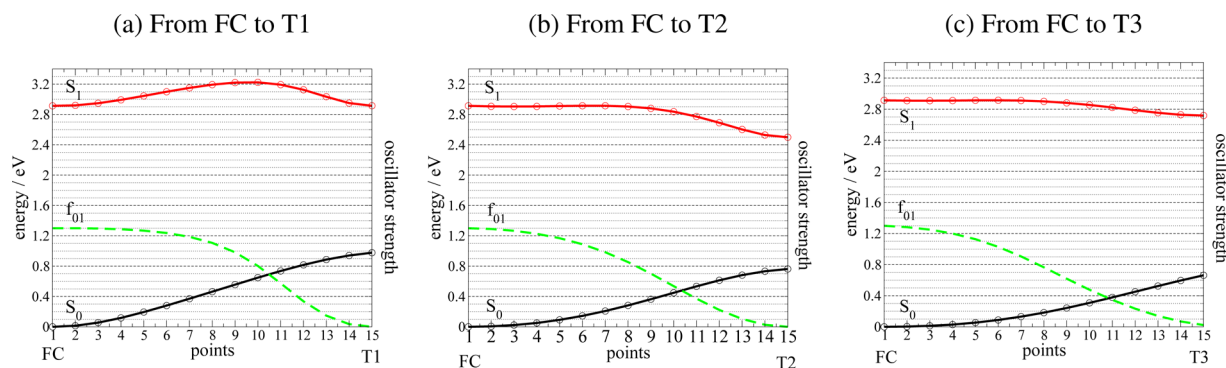

(a) From FC to T1   (b) From FC to T2   (c) From FC to T3

Figure 7. Linear interpolation of internal reaction coordinate (LIIRC) paths between FC and different torsion minima T1, T2, and T3; CAM-B3LYP PES.
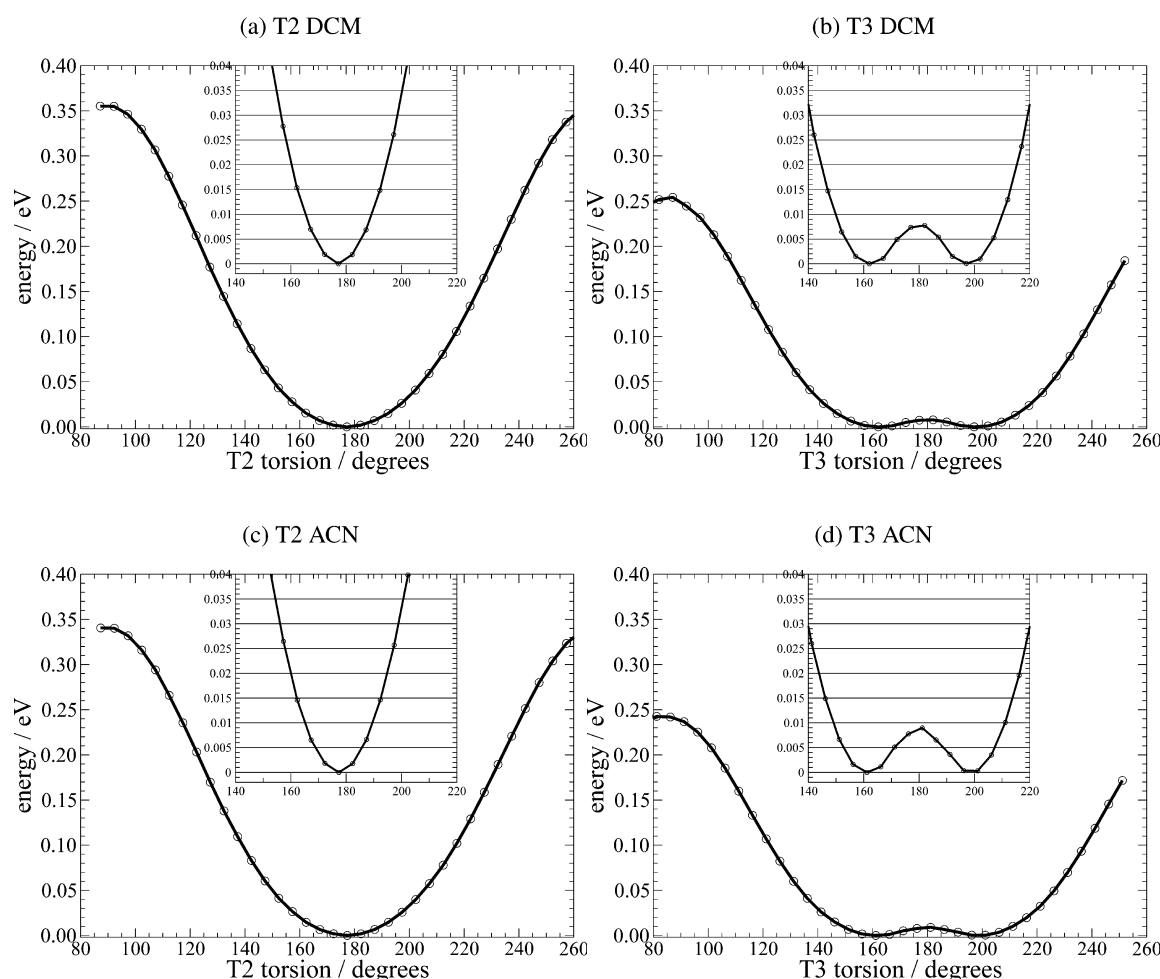
Figure 8. Relaxed CAM-B3LYP/PCM scans around T2 (a, c, e) and T3 (b, d, f) torsions on the GS geometry of DASPMI in two solvents of different polarity, namely, DCM (a, b) and ACN (c, d).

Table 4. SS Vertical Excitation Energies in Eq and Neq Solvatation Regimes for DCM and ACN Solvents with LR Energies Also Reported for ACN in Parantheses

ΔE_{vert} (eV)	FC	LE	T1	T2	T3
			DCM		
GS (eq)	0.00	0.03	0.88	0.65	0.58
S_1 (neq)	3.10	3.09	3.17	2.91	3.00
S_1 (eq)	3.00	2.97	2.02	1.70	1.84
GS (neq)	0.03	0.06	1.27	1.05	0.96
			ACN		
GS (eq)	0.00	0.03	0.87	0.63	0.56
S_1 (neq)	3.17 (2.93)	3.15	3.50 (3.58)	3.28 (3.32)	3.37 (3.51)
S_1 (eq)	3.01 (2.68)	2.99	1.87 (3.58)	1.58 (3.31)	1.77 (3.50)
GS (neq)	0.05	0.08	1.42	1.20	1.10

a much stiffer scanning curve. Another aspect that should be pointed out concerns the presence of two minima of equal energy in the T3 scanning curves with a very low barrier, which slightly increases when passing from DCM to ACN.

Excited States. According to our results, CAM-B3LYP correctly describes the electronic transition of low-lying excited states but quantitatively underestimates the amount of charge transferred in each transition.

Solvent effects for ES are summarized in Table 4. First, let us consider the case of ACN, regarding the relative energies between minima, when the solvent is treated at the SS level, T1,

T2, and T3 are more stabilized by the solvent than the LE state. On the contrary, the LR scheme does not provide any TICT more stable than LE minima; this is in contrast with the gas phase result and the well-accepted picture considering a larger stabilization of ESs with a higher electric dipole moment with respect to those with a lower electric dipole moment when increasing the solvent polarity.

Concerning the solvation regimes in LR, neq and eq regimes give similar energies for TICT minima. On the contrary, by the SS approach, a strong solvent stabilization is observed when going from neq to eq in the twisted minima. Such big

differences between LR and SS approaches could be ascribed to the fact that in the LR approach, the difference between eq and neq solvation energies is proportional to the transition density matrix between the two states, thus vanishing for weak or nonallowed transitions,[50] such as in the case of TICT minima ($f < 0.05$).

LR and SS approaches give significantly different results for DASPMI regarding relative minima energies and the results obtained adopting eq/neq regimes. The intensity of the S_1 electronic transition decreases from $f = 1.2$ (S_1(FC)) to $f \approx 0$ (TICT) in the interval of twisting angles examined. Therefore, DASPMI shows the typical behavior of those systems having a balanced treatment of a covalent minimum (LE) with significant oscillator strength and several TICT minima with negligible transition probability, and thus, this suggests that the study of solvent effects needs the SS treatment.

On the basis of these arguments, a reliable approach to the study of DASPMI photochemistry should deal with the exploration of the ES PES at the gas phase level and the inclusion of the solvent effect with SS-PCM.

On the basis of the results of Table 4 (energy of minima) in DCM, the environment stabilizes the TICT and slightly destabilizes the LE minimum. When passing to the polar solvent (ACN), a remarkable stabilization of the minimum is observed, which turns in an energy gap between LE and TICT for T2 and T3 minima of 1.41 and 1.22 eV, respectively. Thus, T2 and T3 are the most stable minima in solution, and their populations are enhanced in solvents of increasing polarity.

Regarding the deactivation to the GS, the T2 torsion path was computed at the SS level in ACN, and $S1$ PES in eq and with neq solvent regimes were depicted to separate fast and slow dynamics of solvent to analyze how the S_1 and S_0 PES evolve along the torsional motion (see Figure 9). When the
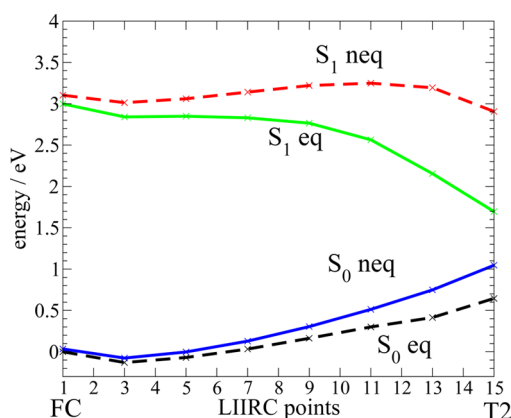

Figure 9. SS S_1 and S_0 energies in equilibrium (eq) and nonequilibrium (neq) regimes in ACN for DASPMI in linear interpolation internal reaction coordinate points between FC and T2 minima.

solvent is fully equilibrated in the T2 minima (S_1(eq)), the S_1−S_0 gap is strongly reduced with respect to the neq regime, which could enhance the twisted deactivation mechanism as a radiationless deactivation path in solvent with increasing polarity.

Overall, the trends of solvent effects are in agreement with earlier observations and with the study of charge localization shown in the Charge Localization section.

■ CONCLUSIONS

Through a detailed exploration of the electronic structure and a careful analysis of the energies, electrostatic properties, and potential energy surfaces of the low lying ESs of DASPMI, we provide new insights into the deactivation mechanism, enhancement of ICT, and shortening of the ES lifetimes in solvents of increasing polarity.

According to our interpretation, we resolve the major questions concerning the uncommon behavior of DASPMI: (a) defining an ICT model, (b) clarifying the multifluorescence emission properties, (c) proposing a specific torsion coordinate, (d) elucidating a radiationless deactivation path, which competes with fluorescence, (e) individuating the charge shift and localization on different electronic states, and (f) clarifying the dependence of the spectroscopic properties on the solvent.

(a) ICT model. The initial absorption populates the FC-LE state; torsional motion paths show that the system evolves from LE via a twisting motion toward twisted ICT S_1 minima. Considering that no planar ICT minimum was found in the S_1 surface, our results validate the two-state model proposed in refs 11 and 25.

(b) Multifluorescence. The twisting deactivation competes with the direct deactivation near FC (LE). One possibility is that the system radiatively decays to the GS, emitting fluorescence; the probability of this decay is not negligible for planar geometries (non-negligible oscillator strength), but the actual occurrence depends on the lifetime of the emitting species. On the basis of the topology of the PES along the twisted path, we suggest that the system evolves along a quite flat PES surface, covering a range of twist angles around which the system could emit because twisted minima are reached and populated. Thus, we related the dynamic asymmetric broadening of fluorescence to the contribution of the twisted structures in the red shift fluorescence.[23]

(c) Specific torsion coordinate. Three kinds of minimum, related to as many twisted rotamers (T1, T2, and T3), are found for S_1. T2 and T3 are the most stable as suggested by Rettig et al.[26] The most stable twisted minimum is T2 in accordance with experimental findings.[31]

(d) Radiationless deactivation. Larger twisting motions were proposed for radiationless deactivation. On the basis of the energy of the minima (T2 and T3 more stable than LE), negligible oscillator strength (low probability of emission) of several twisted minima and the reduction of energy gap between ES and GS along the torsion coordinates, we propose a twisted of twisting along T2 (and, to a lesser extent, along T3) as the radiationless deactivation path. This is in good agreement with assignment of T2 as the main mode of radiationless deactivation.[31]

(e) Charge localization. In the GS, the positive charge is localized on the methyl-pyridinium moiety. After the photoexcitation, the charge delocalizes over the whole molecule and slightly toward the dimethylamino-phenyl moiety. Subsequently, the molecule relaxes via twisting around T2 (in less contribution T3) coordinates, which causes a dynamic transfer of charge to the dimethylaminophenyl moiety (donor moiety). TICT charge localization (positive charge localized on the donor moiety) seems to be in agreement with the previous assignment as reported in ref 26.

(f) Solvent dependence of the dynamics. Spectroscopical properties of DASPMI are strongly dependent in the presence of the solvent. The results show a huge difference between LE

and T2/T3 positive charge localization (in LE, the positive charge is more delocalized than in T2 and T3). This leads to a larger stabilization of T2 and T3 minima with respect to LE in a polar solvent, allowing for a larger population of the twisted forms and enhancement of the TICT population and twisted radiationless deactivation with increasing solvent polarity.

The good agreement between our theoretical results with earlier theoretical and experimental observations supports the hypotheses proposed in this work. Both the asymmetric spectral broadening and the enhanced nonradiative decay thus seem to be caused by the same process, i.e., a twisting motion.

■ ASSOCIATED CONTENT

Ⓢ Supporting Information

The Supporting Information is available free of charge on the ACS Publications website at DOI: 10.1021/acs.jctc.5b00632.

　　CASSCF/CASPT2 methodology, DFT functionals, basis set effects, and minima (PDF)

■ AUTHOR INFORMATION

Corresponding Authors
*Phone: +34 (0) 647927784. Fax: +39 (0)50 563 513. E-mail: mireiasegado@gmail.com.
*Phone: +39 (0) 50509682. E-mail: enrico.benassi@sns.it.

Notes
The authors declare no competing financial interest.

■ ACKNOWLEDGMENTS

■ REFERENCES

(1) Rettig, W.; Strehmel, B.; Schrader, S.; Seifert, H. *Applied Fluorescence in Chemistry, Biology, and Medicine*; Springer, 1998; pp 491–507.

(2) Chemla, D.; Zyss, J. *Non linear optical properties of organic Molecules and Crystals*; Academic Press: Orlando, FL, 1987; Vol. *1 and 2*.

(3) Mishra, A.; Behera, R.; Behera, P.; Mishra, B.; Behera, G. *Chem. Rev.* **2000**, *100*, 1973–2011.

(4) Dekhtyar, M.; Rettig, W. *J. Phys. Chem. A* **2007**, *111*, 2035–9.

(5) Fabian, J.; Nakazumi, H.; Matsuoka, M. *Chem. Rev.* **1992**, *92*, 1197–1226.

(6) Zhao, C. F.; Gvishi, R.; Narang, U.; Ruland, G.; Prasad, P. N. *J. Phys. Chem.* **1996**, *100*, 4526–4532.

(7) Mujumdar, S. R.; Mujumdar, R. B.; Grant, C. M.; Waggoner, A. S. *Bioconjugate Chem.* **1996**, *7*, 356–362.

(8) Ashwell, G.; Jackson, P.; Crossland, W. *Nature* **1994**, *368*, 438–440.

(9) Duan, X.-M.; Konami, H.; Okada, S.; Oikawa, H.; Matsuda, H.; Nakanishi, H. *J. Phys. Chem.* **1996**, *100*, 17780–17785.

(10) Loew, L.; Scully, S.; Simpson, L.; Waggoner, A. *Nature* **1979**, *281*, 497–499.

(11) Fromherz, P.; Dambacher, K. H.; Ephardt, H.; Lambacher, A.; Müller, C.; Neigl, R.; Schaden, H.; Schenk, O.; Vetter, T. *Berichte der Bunsengesellschaft für physikalische Chemie* **1991**, *95*, 1333–1345.

(12) Pierre, A. *Biocatal. Biotransform.* **2004**, *22*, 145–170.

(13) Jóźwik, D.; Miller, E.; Wandelt, B.; Wysocki, S. *Spectrochim. Acta, Part A* **2006**, *64*, 1125–32.

(14) Güsten, H.; Schulte-Frohlinde, D. *Tetrahedron Lett.* **1970**, *11*, 3567–3570.

(15) Gorner, H.; Gruen, H. *J. Photochem.* **1985**, *28*, 329–350.

(16) Sczepan, M.; Rettig, W.; Tolmachev, A. I.; Kurdyukov, V. V. *Phys. Chem. Chem. Phys.* **2001**, *3*, 3555–3561.

(17) Gawinecki, R.; Trzebiatowska, K. *Dyes Pigm.* **2000**, *45*, 103–107.

(18) Wang, H.; Helgeson, R.; Ma, B.; Wudl, F. *J. Org. Chem.* **2000**, *65*, 5862–5867.

(19) Bingemann, D.; Ernsting, N. P. *J. Chem. Phys.* **1995**, *102*, 2691–2700.

(20) Huang, Y.; Cheng, T.; Li, F.; Luo, C.; Huang, C.-H.; Cai, Z.; Zeng, X.; Zhou, J. *J. Phys. Chem. B* **2002**, *106*, 10031–10040.

(21) Sahoo, D.; Chakravorti, S. *Photochem. Photobiol.* **2009**, *85*, 1103–1109.

(22) Letrun, R.; Dekhtyar, M. K. M. L.; Kurdyukov, V. V.; Tolmachev, A.; Rettig, W.; Vauthey, E. *J. Phys. Chem. A* **2013**, *117*, 13112–26.

(23) Ramadass, R.; Bereiter-Hahn, J. *J. Phys. Chem. B* **2007**, *111*, 7681–90.

(24) Benassi, E.; Carlotti, B.; Segado, M.; Cesaretti, A.; Spalletti, A.; Elisei, F.; Barone, V. *J. Phys. Chem. B* **2015**, *119*, 6035–6040.

(25) Ephardt, H.; Fromherz, P. *J. Phys. Chem.* **1989**, *93*, 7717–7725.

(26) Strehmel, B.; Seifert, H.; Rettig, W. *J. Phys. Chem. B* **1997**, *5647*, 2232–2243.

(27) Gómez, I.; Castro, P. J.; Reguero, M. *J. Phys. Chem. A* **2015**, *119*, 1983–1995.

(28) Segado, M.; Carvajal, M.-A.; Gómez, I.; Reguero, M. *Theor. Chem. Acc.* **2011**, *128*, 713–725.

(29) Carlotti, B.; Consiglio, G.; Elisei, F.; Fortuna, C. G.; Mazzucato, U.; Spalletti, A. *J. Phys. Chem. A* **2014**, *118*, 3580–3592.

(30) van der Meer, M.; Zhang, H.; Rettig, W.; Glasbeek, M. *Chem. Phys. Lett.* **2000**, *320*, 673–680.

(31) Martin-Gassin, G.; Villamaina, D.; Vauthey, E. *J. Am. Chem. Soc.* **2011**, *133*, 2358–2361.

(32) Rei, A.; Hungerford, G.; Belsley, M.; Ferreira, M. I. C.; Schellenberg, P. *Int. J. Spectrosc.* **2012**, *2012*, 1–5.

(33) Cammi, R.; Cossi, M.; Mennucci, B.; Tomasi, J. *J. Chem. Phys.* **1996**, *105*, 10556–10564.

(34) Tomasi, J.; Mennucci, B.; Cancès, E. *J. Mol. Struct.: THEOCHEM* **1999**, *464*, 211–226.

(35) Scalmani, G.; Frisch, M. J. *J. Chem. Phys.* **2010**, *132*, 114110–114124.

(36) Mennucci, B. *Wiley Interdisciplinary Reviews: Computational Molecular Science* **2012**, *2*, 386–404.

(37) Peach, M. J. G.; Benfield, P.; Helgaker, T.; Tozer, D. J. *J. Chem. Phys.* **2008**, *128*, 044118–1–044118–8.

(38) Yanai, T.; Tew, D. P.; Handy, N. C. *Chem. Phys. Lett.* **2004**, *393*, 51–57.

(39) Lee, C.; Yang, W.; Parr, R. G. *Phys. Rev. B: Condens. Matter Mater. Phys.* **1988**, *37*, 785–789.

(40) Becke, A. D. *J. Chem. Phys.* **1993**, *98*, 5648–5652.

(41) Adamo, C.; Barone, V. *J. Chem. Phys.* **1999**, *110*, 6158–6170.

(42) Zhao, Y.; Truhlar, D. *Theor. Chem. Acc.* **2008**, *120*, 215–241.

(43) Vydrov, O. A.; Scuseria, G. E. *J. Chem. Phys.* **2006**, *125*, 234109.

(44) Chai, J.-D.; Head-Gordon, M. *J. Chem. Phys.* **2008**, *128*, 084106–084121.

(45) Basis sets of the N07 and SNS families are available for download: http://dreams.sns.it (accessed April, 2013).

(46) Roos, B. O.; Taylor, P. R.; Sigbahn, P. E. *Chem. Phys.* **1980**, *48*, 157–173.

(47) Finley, J.; Malmqvist, P.; Roos, B. O.; Serrano-Andrés, L. *Chem. Phys. Lett.* **1998**, *288*, 299–306.

(48) Krylov, A. I. *Annu. Rev. Phys. Chem.* **2008**, *59*, 433–462.

(49) Daudel, R.; Lefebvre, R.; Moser, C. *Quantum Chemistry. Methods and Applications*; Interscience Publishers Inc.; Cap. IX.: New York, 1959.

(50) Improta, R.; Scalmani, G.; Frisch, M. J.; Barone, V. *J. Chem. Phys.* **2007**, *127*, 074504−074509.

(51) Frisch, M. J.; Trucks, G. W.; Schlegel, H. B.; Scuseria, G. E.; Robb, M. A.; Cheeseman, J. R.; Scalmani, G.; Barone, V.; Mennucci, B.; Petersson, G. A.; Nakatsuji, H.; Caricato, M.; Li, X.; Hratchian, H. P.; Izmaylov, A. F.; et al. *Gaussian 09*, revision D.01; Gaussian Inc.: Wallingford CT, 2009.

(52) Aquilante, F.; de Vico, L.; Ferré, N.; Ghigo, G.; Malmqvist, P.; Neogrády, P.; Pedersen, T. B.; Pitoňák, M.; Reiher, M.; Roos, B. O.; Serrano-Andrés, L.; Urban, M.; Veryazov, V.; Lindh, R. *J. Comput. Chem.* **2010**, *31*, 224−247.

(53) Aidas, K.; Angeli, C.; Bak, K. L.; Bakken, V.; Bast, R.; Boman, L.; Christiansen, O.; Cimiraglia, R.; Coriani, S.; Dahle, P.; Dalskov, E. K.; Ekström, U.; Enevoldsen, T.; Eriksen, J. J.; Ettenhuber, P.; et al. *Wiley Interdiscip. Rev.: Comput. Mol. Sci.* **2014**, *4*, 269−284.

(54) Eriksen, J. J.; Sauer, S. P.; Mikkelsen, K. V.; Christiansen, O.; Jensen, H. J. A.; Kongsted, J. *Mol. Phys.* **2013**, *111*, 1235−1248.